

NISTIR 6588

**FIFTEENTH MEETING OF THE UJNR
PANEL ON FIRE RESEARCH AND SAFETY
MARCH 1-7, 2000**

VOLUME 1

Sheilda L. Bryner, Editor



NIST

**National Institute of Standards and Technology
Technology Administration, U.S. Department of Commerce**

NISTIR 6588

**FIFTEENTH MEETING OF THE UJNR
PANEL ON FIRE RESEARCH AND SAFETY
MARCH 1-7, 2000**

VOLUME 1

Sheilda L. Bryner, Editor

November 2000



U. S. Department of Commerce

Norman Y. Mineta, Secretary

Technology Administration

Dr. Cheryl L. Shavers, Under Secretary of Commerce for Technology

National Institute of Standards and Technology

Raymond G. Kammer, Director

Understanding Sprinkler Sprays: Trajectory Analysis

DAVID T. SHEPPARD and PRAVINRAY D. GANDHI, Ph.D.
Underwriters Laboratories, Inc.
Northbrook, IL USA

RICHARD M. LUEPTOW, Sc.D.
Northwestern University
Evanston, IL USA

1 Abstract

Previous research on the characterization of sprinkler water spray has concentrated on understanding the droplet and velocity size distributions. However, previous research appears not have used the droplet and velocity distributions to determine the delivered density of water at a specific distance below the sprinkler, and thus the results, while interesting, do not provide an analysis of the local delivered density. This is an important factor in control and suppression of fires.

In this paper, an analytical trajectory analysis is combined with the results of experiments conducted with a laser measurement technique called Particle Image Velocimetry (PIV). The trajectory analysis is used to predict the path of individual droplets. Particle Image Velocimetry (PIV) is used to develop a description of the droplet velocities and water densities leaving the sprinkler.

The trajectory analysis provided several insights into the physics of sprinkler sprays. For example, it was found that larger droplets always travel farther horizontally from the sprinkler than smaller droplets. This phenomena is caused by the momentum of larger droplets being proportionally larger than the drag force.

The experimental study has shown that the droplet velocities and water fluxes are different at different angles from the sprinkler. It was found that, for the sprinkler studied, the droplet velocities could be characterized as a purely radial flow at a radial distance ranging from 175 to 300 mm depending on the sprinkler. Further, it was also found that the angular dependence of the spray characteristics produce different delivered water densities and that the sprinkler sprays can not be characterized as axisymmetric flows.

The combination of the trajectory analysis and the experimental study was used to predict the water density measured in the traditional pan distribution tests. The results of this comparison provided good preliminary results. Further refinement of the analysis and experimental techniques will be required to provide acceptable engineering results.

2 Measurement Techniques

2.1 Sprinkler Spray Characterization Experiments

Particle Image Velocimetry (PIV) is used for characterizing the sprinkler spray velocity distributions and water fluxes. In PIV a sheet of high-intensity laser light is positioned within the flow field. A video camera is aligned perpendicular to the laser sheet so that it can image the droplets when they are illuminated by a flash of laser light that is only a few nanoseconds long as shown in Figure 1. Using a sequential pair of images of droplets, the statistical average of the displacement of many droplets in the same region of the imaged velocity field is determined using Fourier-based cross-correlation methods. In this way, a grid of velocity vectors for the droplets in the plane of the laser sheet can be determined simultaneously.

2.2 Water Distribution

Ten pan tests are conducted using one sprinkler located above a rotating array of pans as shown in Figure 2. Ten pan tests provide a measure of the delivered water density as a function of radial distance from the fire. Test

parameters that are typically changed in pan distribution tests are the height of the sprinklers above the pans and the water flow rate at the sprinkler.

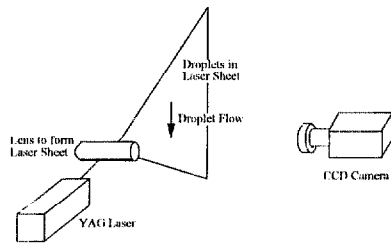


Figure 1. Sketch of PIV setup

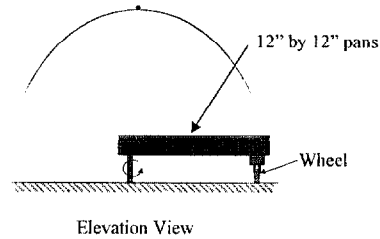


Figure 2. Pan Distribution Tests

3 Analysis Techniques

3.1 Droplet Trajectory

Water from sprinklers ejects from a circular orifice to form a water jet. The water jet impacts against a deflector and disperses in a thin sheet or thin streams called ligaments, which break up into droplets due to surface tension and inertial forces. [1]

The trajectories of the droplets may be analyzed once the stable droplets are formed. Assuming that this happens a short distance away from the deflector and that the droplets are spherical in shape once formed, the trajectory of droplets may be described with the analysis of forces on a sprinkler drop as depicted in Figure 3.

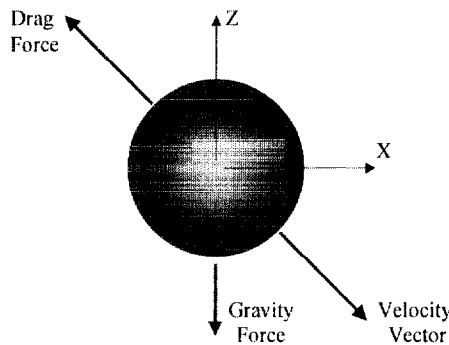


Figure 3 – Forces on a Sprinkler Spray Drop

These forces may be used to describe the force balance as shown in equation (1.1). In this equation, the left hand side represents the change in momentum of the drop. The first term on the right hand side is the force of gravity on the droplet and the second term is the drag force that the surrounding air exerts on the droplet [2].

$$\frac{\partial}{\partial t}(m_d \bar{u}_d) = m_d \bar{g} - \frac{1}{2} \rho C_d A_d (\bar{u}_d - \bar{u}_\infty) |\bar{u}_d - \bar{u}_\infty| \quad (1.1)$$

Here m_d is the mass of the droplet, g is the acceleration due to gravity, ρ is the density of water, A_d is the projected area of the droplet, C_d is the drag coefficient, u_d is the velocity of the droplet and u_∞ is the velocity of the surrounding air. The quantities g , u_d and u_∞ are vectors.

The drag coefficient, C_d , for spheres can be found in the literature [3] to be a function of the Reynolds Number as shown in equation (1.2).

$$C_d = \frac{24}{Re} + \frac{6}{1 + \sqrt{Re}} + 0.4 \quad (1.2)$$

The trajectory of individual droplets was calculated by solving equation (1.1) using a 4th order Runge-Kutta algorithm. The velocity of the ambient air was always assumed to be zero. The initial velocity vector and the droplet diameter were user-defined input variables. The velocity vector was allowed to change in response to the solution of equation (1.1). The droplet size was assumed to remain constant.

3.2 Delivered Water Density Based on Droplets near the Sprinkler

The effectiveness of a sprinkler in controlling a fire depends on the amount of water that the sprinkler can deliver to the fire location. When water spray characteristics are known near the sprinkler, it should be possible to calculate the delivered water density at any location. This calculation is made challenging because of the large number of water droplets and because the droplet sizes, droplet velocities, and water fluxes are different at different angles from the sprinkler.

Because the sprinkler spray is not immediately a fully developed droplet flow (i.e. droplets are still forming and changing shape and size), the measurement of sprinkler spray characteristics must be made at a distance away from the sprinkler. For this reason, the droplet flow has been evaluated by modeling the sprinkler as existing at the center of a spherical region as shown in Figure 4.

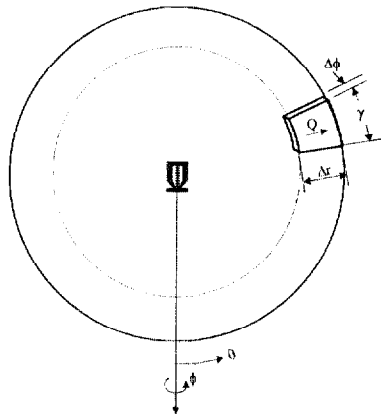


Figure 4. Sprinkler Located at center of Sphere

The experimental measurements are mapped into differential volumes as shown in Figure 4. The velocity, droplet sizes, and water flux are assumed to be uniform within each differential volume and are allowed to have different values in different volumes.

Using the measured droplet sizes and velocities obtained using PIV, the water distribution at a plane below the sprinkler can be calculated as follows. The droplet density in a differential volume is calculated from the area of droplets measured in the PIV images. The measured flow rate in a differential volume, Q , is calculated from the product of the average droplet velocity in a differential volume (from PIV), the differential volume, and the droplet density in the volume. The water flux at any plane below the sprinkler is calculated by distributing the measured flow rate in the differential volume, Q , evenly over the area bounded by the trajectories of the droplets at the boundaries of the pie shaped differential volume in Figure 4. The sum of the contributions of all of the individual differential volumes at a plane below the sprinkler provides the water distribution based on the droplet sizes and velocities near the sprinkler. This result can then be compared to the results for large scale water distribution tests.

Several assumptions used in this analysis should be noted. First, the droplet velocity and water flux are assumed to be functions of elevation angle θ and azimuthal angle ϕ . Second, the droplet spray is assumed to be adequately described in 10 degree increments of θ . It is also assumed that the spray has uniform characteristics for ϕ ranging from 30 to 90 degrees, where 0 degrees is parallel to the frame arms. Third, the droplet size distribution near the sprinkler is assumed to be independent of location. This assumption is clearly invalid due to the effects of the frame

arms and irregularly shaped deflectors. The droplet distribution data was also not measured for the sprinklers used. The droplet distribution is assumed to follow a Rosin-Rammler distribution with an identical median diameter and distribution function for all angles. Finally, we have assumed that the interaction between the droplets does not significantly effect the flow.

4 Results

4.1 Trajectory Analysis

A trajectory analysis was conducted to determine the path of individual droplets ejected from a sprinkler. The purpose of the trajectory analysis was to develop a fundamental understanding of the spray characteristics that were observed in the experimental tests. The trajectories of the droplets were calculated using the procedure outlined in section 3.1.

The analysis consisted of calculating the radial distance from the centerline of the sprinkler that a droplet would reach when it has fallen 3 meters below the sprinkler. Droplet diameters ranged from 50 to 7000 microns, initial droplet velocities ranged from 0 to 20 meters per second, and initial velocity angles, θ , ranged from 60 to 110 degrees.

Results for the case where droplets are ejected horizontally from the sprinkler, $\theta = 90$ degrees, are shown in Figure 5. The figure indicates the size of the droplet that lands at a given radial distance from the sprinkler centerline on a horizontal plane 3 meters below the sprinkler, given a particular initial velocity. For instance, 600 micron droplets with an initial velocity of 2 m/s will land on a plane 3 meters below the sprinkler at about 1 meter from the sprinkler centerline. Data is shown in Figure 5 for initial velocities ranging from 2 to 20 m/s and droplet diameters of 100 to 1200 microns.

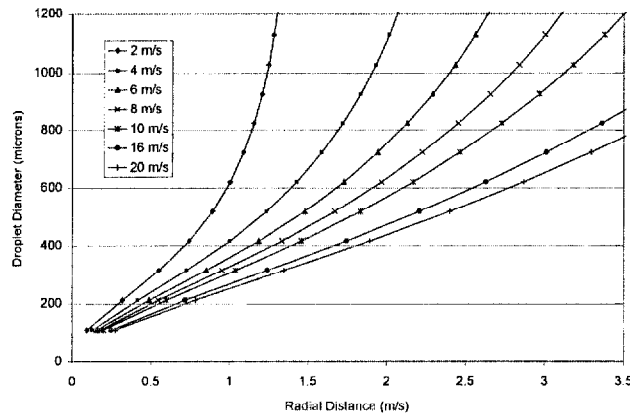


Figure 5. Droplet Size Versus Radial Position (numerical solution)

It is evident that larger droplets travel further radially than smaller droplets regardless of the initial horizontal velocity. At low initial velocities, the difference in the distance that the largest and smallest droplets travel is much less than the difference at larger initial velocities.

The tendency for larger droplets to travel further horizontally than smaller droplets was found for all initial velocities and angles in this study. A similar result was found experimentally by Chan [4] for three ESFR sprinklers. Likewise, Phased Doppler Particle Analyzer measurements at Underwriters Laboratories show the same result.

4.2 Experiments

Experimental results presented here are for a Grinnel Model FR-1 sprinkler with a nominal orifice coefficient of $k=5.5 \text{ gpm}/(\text{psi})^{1/2}$. Experiments were conducted at a nominal flow rate of 57 LPM (15 gpm). Four series of

experiments were conducted with the sprinkler frame arms parallel, 10, 20, and 30 degrees from the PIV laser sheet, corresponding to $\phi=0, 10, 20,$ and 30 degrees.

In each sprinkler orientation, one hundred PIV image pairs were collected with a 0.3 millisecond interval between each frame of an image pair. Image pairs were taken with a 66 millisecond separation. The resolution of the PIV images was 0.294 mm/pixel in a 1000 by 1000 pixel image for a total image area of 294 by 294 mm (11.6 by 11.6 inches).

Figure 6 shows PIV generated velocity vectors superimposed over the PIV image. The sprinkler is located in the upper left-hand corner of the image. The water jet is clearly visible between the two sprinkler frame-arms. Water ligaments hide the deflector. The image shows that the majority of the water ligaments have broken up into droplets by about 100 mm from the sprinkler. The image clearly shows that the water density is non-uniform with respect to elevation angle θ .

4.3 Droplet Velocities

The radial velocity of the droplets was calculated using the following procedure. The average droplet velocity for each location on a 13 by 13 uniform grid for the 100 image pairs was calculated after first removing any vector that was more than 3 standard deviations from the median in that grid location. The radial and angular components of velocity were calculated using the center of the orifice as the origin and using a linear interpolation to find velocities at locations not on the 13 by 13 grid. The origin was then shifted vertically to find the location with the minimum angular velocity components. This resulted in a virtual origin location between the orifice and the deflector, though closer to the orifice. After locating the virtual origin, the radial velocities were at least 20 times larger than angular velocities except in the regions with small velocity.

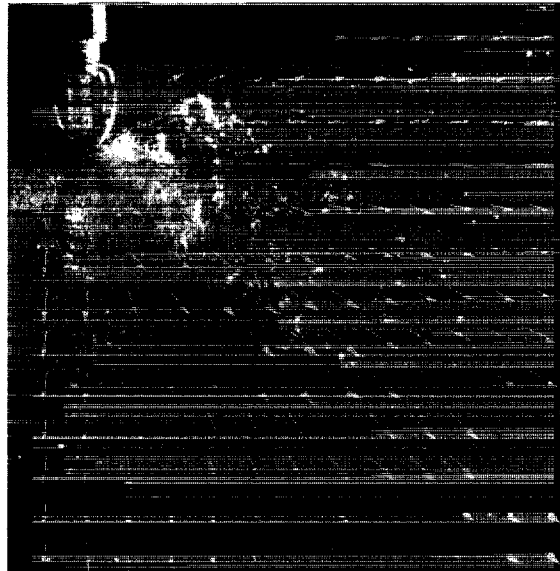


Figure 6. PIV Image

Figure 7 shows the radial velocity on a circle 200 mm from the virtual origin. The radial velocity is plotted on the vertical axis as a function of the elevation angle, θ , from the vertical axis (ranging from 0 directly below the sprinkler to 90 degrees directly to the side of the sprinkler). The droplet velocity ranges from 3.7 to 8.2 m/s. The four series in the Figure represent the four sprinkler azimuthal orientations in the ϕ direction.

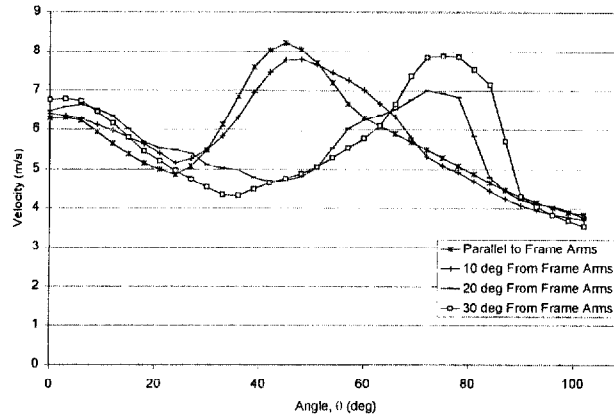


Figure 7. Droplet Radial Velocity at a 200mm Radial Distance from Sprinkler

It is evident that the droplet velocity is a function of both the elevation angle θ and the azimuthal angle ϕ . Figure 7 also shows that the velocities parallel to the frame arms and at 10 degrees from the frame arms are similar one another. Likewise the velocities at 20 and 30 degrees to the frame arms are similar. This suggests that the frame arm effect on the velocity profile dies out between 10 and 20 degrees.

4.4 Water Flux

Figure 8 shows the water flux leaving the sprinkler that was calculated from the PIV images using the procedure outlined in section 3.2. The Figure shows the water flux as a function of the elevation angle, θ , from the vertical axis. The droplet density was calculated in 3 degree wide regions that were bounded by the radial distances of 175mm to 225 mm from the origin. The virtual origin calculated in section 4.3 was used.

Clearly the greatest water flux for this sprinkler is directly below the sprinkler at all azimuthal angles. For planes parallel or nearly parallel to the frame arms, the flux is also highest around 45 degrees. Away from the frame arm, a higher water flux occurs at greater angles. It is important to note that although the water flux is quite large directly below the sprinkler, the effect of this is fairly small when integrated over the spherical region shown in .

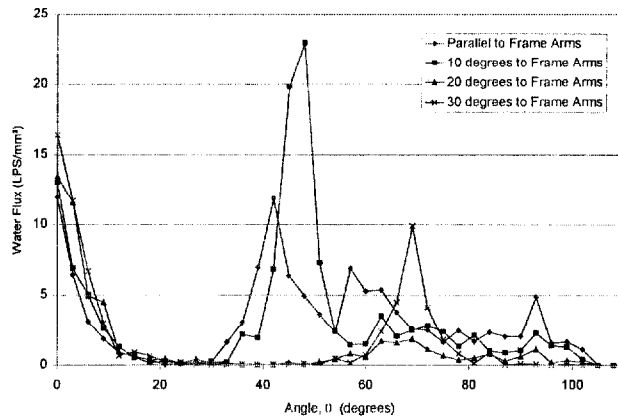


Figure 8. Water Flux

4.5 Delivered Water Density

Figure 9 shows the delivered water density on a plane 3m below the sprinkler that would be calculated if the spray could be treated as an axisymmetric flow. In other words, each chart in Figure 9 shows the calculated water density as if the spray characteristics at each sprinkler angle, ϕ , could be assumed to be characteristic of the entire spray.

Figure 9 demonstrates that the spray characteristics at each sprinkler angle, ϕ , produce different delivered water densities and that the sprinkler sprays can not be characterized as axisymmetric flows.

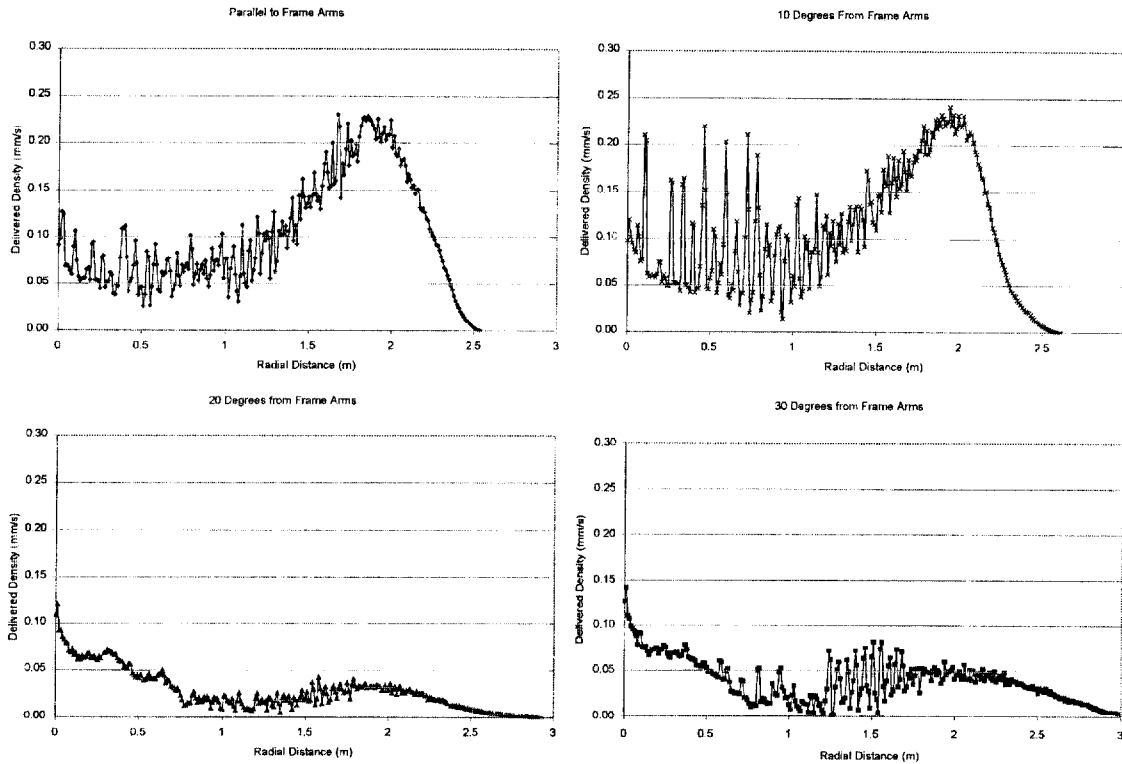


Figure 9. Calculated Delivered Water Density for Each Sprinkler Orientation

The delivered water densities calculated for each sprinkler angle, ϕ , were then combined to produce a composite delivered water density. The spray was assumed to be quadrilaterally-symmetric. That is, the spray in each azimuthal quadrant is assumed to be similar. The delivered density from the experiment parallel to the frame arms was assumed to contribute 5/90 of the delivered density. The delivered density from the experiments 10 and 20 degrees from the frame arms were each assumed to contribute 10/90 of the delivered density. The delivered density from the experiment at 30 degrees from the frame arms was assumed to contribute 65/90 of the delivered density. The resulting delivered water density is shown in Figure 10.

The composite delivered density shows characteristics of each of the individual experiments. The peak below the sprinkler is due to the influence of the experiments at ϕ values of 20 and 30 degrees. The rise that occurs at 2 meters is primarily due to the influence of the experiments at ϕ values of 0 and 10 degrees.

4.6 Comparison with 10-Pan Distribution Data

Figure 11 shows the results of two 10-pan distribution tests. The results show that there is a peak directly below the sprinkler, a minimum at 0.5 m, and another maximum at 1m. Comparison of Figure 10 and Figure 11 shows that the general shape of the curves is similar. The calculated water distribution extends further than the 10-pan data. The water distribution in the pan tests reduces to trace amounts at distances greater than 2.2m, whereas the calculated water distribution does not reduce to trace amounts until 2.8m. The magnitude of the delivered density in both Figures is similar. The magnitude of the data in the calculated water distribution is less due to the larger area the sprays at a larger distance must cover.

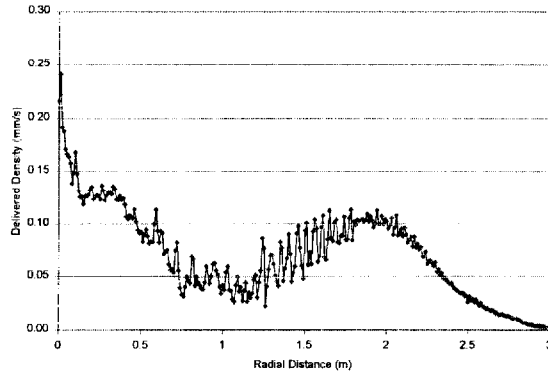


Figure 10. Composite Water Density

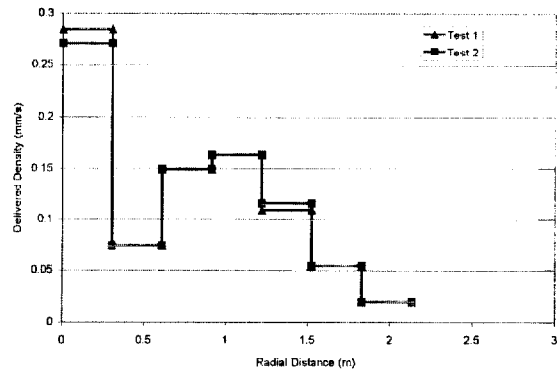


Figure 11. Pan Distribution Results

5 Conclusion

In this paper, an analytical trajectory analysis was combined with Particle Image Velocimetry experiments. The trajectory analysis was used to predict the path of individual droplets. Particle Image Velocimetry (PIV) was used to develop the input parameters at the sprinkler needed for the trajectory analysis.

The trajectory analysis showed that larger droplets always travel farther horizontally from the sprinkler than smaller droplets. This phenomena is caused by the momentum of larger droplets being proportionally larger than the drag force.

The experimental study has shown that the droplet velocities and water fluxes are different at different angles from the sprinkler. For the sprinklers evaluated, it was found that the droplet velocities could be characterized as a purely radial flow at a radial distance of 200 mm. Droplet velocities up to 8.2 m/s were measured from a $k=5.5 \text{ gpm}/(\text{psi})^{1/2}$ flowing water at 15 gpm.

The combination of the trajectory analysis and the experimental study was used to predict the water density measured in the traditional pan distribution tests. The results of this comparison provided good preliminary results. Further refinement of the analysis and experimental techniques will be required to provide acceptable engineering results.

Acknowledgements

The authors would like to acknowledge the National Institute of Standards and Technology for funding this effort and Underwriters Laboratories for providing the facilities.

References

- 1 Joseph M. Prah1 and Bruce Wendt, "Discharge distribution performance for an axisymmetric model of a fire sprinkler head," Fire Safety J. Vol 14, 101-111 , 1988.
- 2 McGrattan, K.B., Baum, H.R., Rehm, R.G., Large Eddy Simulation of Fire Phenomena, National Institute of Standards and Technology, Gaithersburg, MD, 1998.
- 3 White, Frank M., Viscous Fluid Flow, 2nd Ed., MCGraw Hill, Inc., New York. 1991.
- 4 Tak-Sang Chan, Measurements of Water Density and Drop Size Distributions of Selected ESFR Sprinklers, Journal of Fire Protection Engineering, Vol. 6(2), pp. 79-87, (1994).